

# MamMIL: Multiple Instance Learning for Whole Slide Images with State Space Models

Zijie Fang<sup>1</sup>, Yifeng Wang<sup>2</sup>, Zhi Wang<sup>1</sup>, Jian Zhang<sup>3</sup>, Xiangyang Ji<sup>4</sup>, and Yongbing Zhang<sup>5</sup>

<sup>1</sup> Tsinghua Shenzhen International Graduate School, Tsinghua University, Shenzhen 518055, China

<sup>2</sup> School of Science, Harbin Institute of Technology (Shenzhen), Shenzhen 518055, China

<sup>3</sup> School of Electronic and Computer Engineering, Shenzhen Graduate School, Peking University, Shenzhen 518055, China

<sup>4</sup> Department of Automation, Tsinghua University, Beijing 100084, China

<sup>5</sup> School of Computer Science and Technology, Harbin Institute of Technology (Shenzhen), Shenzhen 518055, China

**Abstract.** Recently, pathological diagnosis, the gold standard for cancer diagnosis, has achieved superior performance by combining the Transformer with the multiple instance learning (MIL) framework using whole slide images (WSIs). However, the giga-pixel nature of WSIs poses a great challenge for the quadratic-complexity self-attention mechanism in Transformer to be applied in MIL. Existing studies usually use linear attention to improve computing efficiency but inevitably bring performance bottlenecks. To tackle this challenge, we propose a MamMIL framework for WSI classification by cooperating the selective structured state space model (i.e., Mamba) with MIL for the first time, enabling the modeling of instance dependencies while maintaining linear complexity. Specifically, to solve the problem that Mamba can only conduct unidirectional one-dimensional (1D) sequence modeling, we innovatively introduce a bidirectional state space model and a 2D context-aware block to enable MamMIL to learn the bidirectional instance dependencies with 2D spatial relationships. Experiments on two datasets show that MamMIL can achieve advanced classification performance with smaller memory footprints than the state-of-the-art MIL frameworks based on the Transformer. The code will be open-sourced if accepted.

**Keywords:** Multiple instance learning · State space models · Whole slide images.

## 1 Introduction

As the gold standard for cancer diagnosis, pathology has been undergoing a new leap from manual observation to digital analysis since the approval of whole slide images (WSIs) [1,7]. Accompanied by the growth of deep learning, a new interdisciplinary field, computational pathology, has emerged and attracted tense

attention for modern healthcare [24]. In computational pathology, deep learning-based models are developed to classify WSIs for automatic diagnosis, which largely frees the work burden for pathologists and alleviates the subjectivity in the diagnosis process [13,4].

However, WSIs are composed of tens of billions of pixels, which greatly challenges computational pathology. On the one hand, the tremendous pixels in WSIs hinder the acquisition of fine annotations, which not only require specialized knowledge but also are very time-consuming and expensive. Therefore, only WSI-level labels can be obtained commonly [20]. On the other hand, feeding the huge-sized WSIs into deep learning models is often infeasible due to memory limitations in the graphic processing units (GPUs).

To solve the above issues, researchers have recently paid much attention to multiple instance learning (MIL) for computational pathology [9]. MIL treats each WSI as a bag composed of small patches split from the WSI, called instances. In MIL, feature learning is no longer performed on the giga-pixelated WSIs. Instead, feature extraction is conducted on each small instance, thus solving the problem of GPU memory limitation. After instance feature extraction, MIL aggregates all the instance features to obtain a bag feature, which can be supervised by the WSI-level label, enabling the model training process.

Since the instance aggregation directly affects the discriminability of the bag features and hence determines the model’s performance, many MIL frameworks focus on the aggregation process. For example, Ilse et al. [14] proposed ABMIL, which utilized a gated attention mechanism for instance aggregation. To avoid performance degradation caused by wrong attention, Shi et al. [23] proposed the LossAttn framework. Lu et al. [19] proposed CLAM with a clustering constraint for the instances to alleviate the model’s requirements on large-scale data. To ease the overfitting problem caused by the limited number of training WSIs, Zhang et al. [27] proposed a pseudo-bag strategy and designed DTFDMIL. To address the decision boundary shifting issue caused by the imbalance of negative and positive instances, Li et al. [15] proposed the DSMIL framework.

However, all the above studies assume the instances are independent of each other, i.e., follow an independent and identical distribution (i.i.d.). In contrast, interactions among tissues are critical in tumor progression. For this reason, Shao et al. [22] proposed TransMIL, which utilized Transformer [25] with self-attention to model the pair-wise instance dependencies. However, directly feeding the giga-pixelated WSIs with tens of thousands of instances into the Transformer usually leads to out-of-memory issues due to the quadratic complexity of self-attention, which impedes the model training process. To this end, Transformer-based MIL methods usually approximate self-attention with linear attention, such as Nyströmformer [26]. However, studies show that the performance of linear attention is inevitably limited compared with self-attention [6].

To address the issues in Transformer-based MIL methods, some researchers applied state space models (SSMs) into the MIL framework due to their ability to model long sequences with linear or near-linear complexity. For example, Fillioux et al. [8] utilized an SSM named S4D [11] for MIL. However, the parameters of

S4D are input-invariant, which hinders the model from focusing on the most discriminative instances, leading to inferior performance [10]. Besides, complex-valued parameters are necessary for S4D to obtain satisfactory results, which inevitably increases the GPU memory footprints.

Recently, a new kind of SSM, Mamba [10], has emerged. Compared with previous SSMs suffering from limited performance and increased memory footprint, Mamba extends the SSM’s parameters to a content-dependent manner with real values. Existing studies verified that Mamba can achieve comparable or better performance than Transformer for both natural language processing and visual tasks [10,28,18,21]. However, no studies have utilized Mamba for WSI classification or incorporated it with the MIL framework. All the above reasons motivate us to apply Mamba to MIL for automatic pathology diagnosis with WSIs.

However, several challenges exist in applying Mamba to MIL for WSI classification. Firstly, Mamba is built for one-dimensional (1D) sequences. When flattening the 2D WSIs to 1D sequences as inputs, the loss of 2D spatial information inevitably occurs. Secondly, Mamba uses a “scanning” strategy to compute the latent states in a unidirectional manner. Although unidirectional scanning is feasible to model sequences with a time series characteristic, it may be inefficient for WSIs with bidirectional pair-wise dependencies. To fully utilize Mamba’s ability of long sequence modeling while addressing the above challenges, we propose a MIL framework dubbed MamMIL. Specifically, the main contributions of this paper are listed as follows.

- As a linear-complexity model with comparable performance to Transformer, Mamba is first adopted in this paper to the MIL framework for the WSI classification task, where each bag consists of tens of thousands of instances.
- We introduce a bidirectional SSM block to resolve the unidirectional modeling problem in Mamba. In addition, a 2D context-aware block is employed to avoid the loss of 2D spatial information in 1D sequences.
- Experiments on two datasets prove that MamMIL outperforms SOTA methods while obtaining a lower GPU memory footprint than Transformer-based MIL frameworks. Our work provides a new architecture and direction for future MIL studies.

## 2 Methodology

### 2.1 Framework Overview

Fig. 1 shows an overview of MamMIL, which mainly consists of an instance feature extraction stage and an instance feature aggregation stage. In the first stage, a sliding window is utilized to split WSIs into small, non-overlapping patches as instances. Then, a pre-trained ResNet50 [12] is adopted to extract the instances’ features. After a trainable linear projection with a ReLU activation, the instance features constitute a 1D sequence with a class token appended at the last position. Then, the sequence is fed into the second stage, which consists of a series of stacked MIL-SSM modules. Each MIL-SSM module is composed of

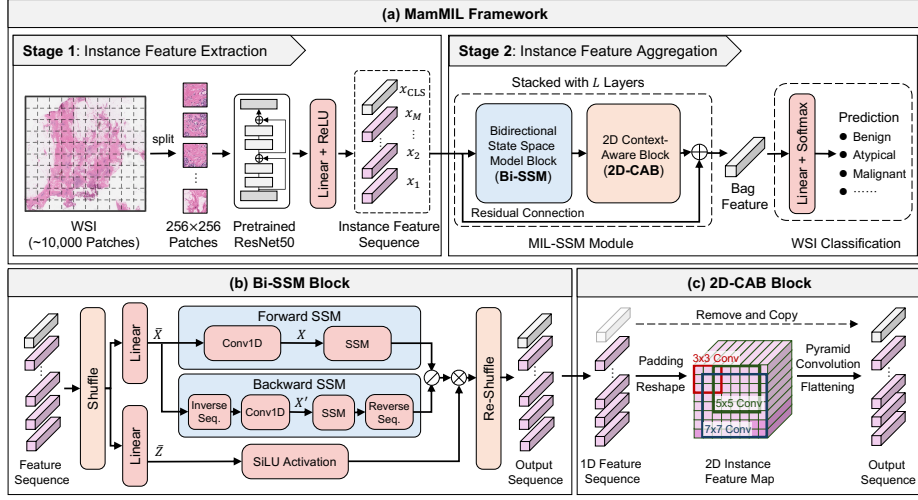


**Fig. 1.** An overview of the MamMIL framework, which is composed of an instance feature extraction stage and an instance feature aggregation stage.  $\oslash$ ,  $\oplus$  and  $\otimes$  represent element-wise averaging, addition, and multiplication, respectively.

a bidirectional SSM (Bi-SSM) block and a 2D context-aware block (2D-CAB). Finally, the class token is utilized as the bag feature for WSI classification.

## 2.2 Instance Feature Extraction

Denote a WSI as  $X$ , we first split the WSI into  $M$  patches (i.e., instances)  $\{p_i\}_{i=1}^M$ , where  $p_i \in \mathbb{R}^{H \times W \times 3}$ . Here,  $H$  and  $W$  represent the height and width of each patch, and  $H = W = 256$ . Next, we utilize an ImageNet [5] pre-trained ResNet50 followed by a trainable linear layer with a ReLU activation  $\mathcal{E}$ , to extract the patch features by  $x_i = \mathcal{E}(p_i) \in \mathbb{R}^{512}$ . After feature extraction, a WSI can thus be represented by a 1D sequence of instance features, i.e.,  $X = \{x_i\}_{i=1}^M$ . Finally, we add a trainable class token  $x_{CLS}$  at the end of the sequence, i.e.,  $X = [x_1, x_2, \dots, x_M, x_{CLS}]$ , which is fed into the next stage for aggregation.

## 2.3 Instance Feature Aggregation

As an essential stage where the instance dependencies are modeled to obtain the bag feature, the instance feature aggregation stage in MamMIL consists of  $L$  stacked MIL-SSM modules, each of which is composed of a Bi-SSM and a 2D-CAB block with a residual connection. Next, the two blocks will be described.

**Bi-SSM Block** In MamMIL, the Bi-SSM block is a key component that utilizes Mamba to quickly mine the discriminative dependencies among the vast number of instances with linear complexity. The main purpose of Mamba is to learn a

mapping from the input instance sequence  $X = \{x_i\}_{i=1}^M$  to an output sequence  $\{y_i\}_{i=1}^M$  through latent states  $\{h_i\}_{i=1}^M$ , which are modeled by

$$h_i = \bar{\mathbf{A}}h_{i-1} + \bar{\mathbf{B}}x_i, \quad y_i = \bar{\mathbf{C}}h_i. \quad (1)$$

In practice, a discretization is required to apply Eq. (1) in deep learning models with discrete inputs and weights. Commonly, like in Mamba,  $\bar{\mathbf{A}}$ ,  $\bar{\mathbf{B}}$ , and  $\bar{\mathbf{C}}$  are discretized by the zeroth-order hold rule with a time step  $\Delta$  as

$$\bar{\mathbf{A}} = \exp(\Delta\mathbf{A}), \quad \bar{\mathbf{B}} = (\Delta\mathbf{A})^{-1}(\exp(\Delta\mathbf{A}) - \mathbf{I}) \cdot \Delta\mathbf{B} \approx \Delta\mathbf{B}, \quad \bar{\mathbf{C}} = \mathbf{C}, \quad (2)$$

where  $\mathbf{A}$ ,  $\mathbf{B}$ ,  $\mathbf{C}$ , and  $\Delta$  are learnable parameters. To enhance the context-perceiving ability, Mamba correlates parameters  $\mathbf{B}$ ,  $\mathbf{C}$ , and  $\Delta$  with the input sequence  $X$  based on three learnable linear projections  $l_{\mathbf{B}}$ ,  $l_{\mathbf{C}}$ , and  $l_{\Delta}$  by

$$\mathbf{B} = l_{\mathbf{B}}(X), \quad \mathbf{C} = l_{\mathbf{C}}(X), \quad \Delta = \log(1 + \exp(l_{\Delta}(X) + \mathbf{P}_{\Delta})), \quad (3)$$

where  $\mathbf{P}_{\Delta}$  represents the learnable parameters for  $\Delta$ .

However, from Eq. (1), we can see that the latent state  $h_i$  is only related to previous latent states and the current input, making  $h_i$  calculated in a unidirectional ‘‘scanning’’ manner. Nevertheless, dependencies between any instances may exist in WSIs. To address this issue, inspired by ViM [28], we construct two SSMs to simultaneously model the forward and backward sequence directions and build the Bi-SSM block. For the forward SSM, we directly feed  $X$  to the SSM and get the output  $Y$ . For the backward SSM, we first invert the instance feature sequence while fixing the class token at the last position to construct  $X'$ . Then,  $X'$  is fed into another SSM to get the output  $Y'$ . Finally, we revert the instance feature part of  $Y'$  and obtain the output of the backward SSM.

To fuse the outputs of the two SSMs, we adopt a gating mechanism. For an input sequence  $X^{(l)}$  of the  $l$ -th MIL-SSM module, we first shuffle  $X^{(l)}$  while fixing the position of the class token to alleviate overfitting. Then, the shuffled  $X^{(l)}$  is fed into two linear projections to get the outputs  $\bar{X}$  and  $\bar{Z}$ . After inverting  $\bar{X}$  and getting  $\bar{X}'$ ,  $\bar{X}$  and  $\bar{X}'$  are respectively fed into a 1D convolution to obtain  $X$  and  $X'$ , which are utilized as the input of the forward or backward SSM. Meanwhile,  $\bar{Z}$  is activated by the SiLU function and employed to gate the average of the two SSMs’ outputs by element-wise multiplication. Finally, the gated sequence is re-shuffled back as the output of Bi-SSM.

**2D Context-Aware Block** Since the Bi-SSM is performed on a 1D sequence, the 2D spatial relationships in the instances still cannot be perceived. To address this problem, we introduce the 2D-CAB based on convolutions with a pyramid structure. Specifically, we first remove the class token and reshape the remaining 1D feature sequence into a 2D squared feature map. In case the number of instances is not divisible, we first cyclically pad the sequence to the nearest perfect square. Then, the 2D spatial relations are extracted with  $3 \times 3$ ,  $5 \times 5$ , and  $7 \times 7$  depth-wise convolutions. The output  $X''$  is obtained by summing the convolution results with a residual connection. Finally,  $X''$  is flattened back to

**Table 1.** Comparison results of MamMIL and SOTA frameworks. The **best results** (mean<sub>std</sub>, %) are bold in red, and the second best results are underlined in blue.

Method	Camelyon16			BRCAS		
	Accuracy	F1-Score	AUC	Accuracy	F1-Score	AUC
ABMIL [14]	77.91 <sub>3.66</sub>	76.42 <sub>3.49</sub>	81.81 <sub>2.41</sub>	<b>66.09</b> <sub>2.63</sub>	<u>58.79</u> <sub>6.15</sub>	<u>82.27</u> <sub>1.64</sub>
CLAMSB [19]	73.06 <sub>3.07</sub>	71.77 <sub>2.57</sub>	79.26 <sub>3.35</sub>	61.78 <sub>0.95</sub>	53.43 <sub>3.95</sub>	80.81 <sub>1.87</sub>
CLAMMB [19]	80.43 <sub>1.68</sub>	77.86 <sub>1.81</sub>	78.69 <sub>2.78</sub>	60.63 <sub>2.62</sub>	51.83 <sub>4.14</sub>	80.10 <sub>1.98</sub>
DSMIL [15]	72.29 <sub>3.26</sub>	68.50 <sub>2.92</sub>	72.44 <sub>4.76</sub>	62.93 <sub>3.29</sub>	53.40 <sub>4.23</sub>	77.73 <sub>1.63</sub>
LossAttn [23]	<u>80.81</u> <sub>1.49</sub>	78.17 <sub>0.96</sub>	76.98 <sub>0.84</sub>	62.07 <sub>1.41</sub>	55.90 <sub>3.87</sub>	79.63 <sub>0.37</sub>
TransMIL [22]	80.04 <sub>3.40</sub>	<u>78.57</u> <sub>3.33</sub>	<u>82.78</u> <sub>3.71</sub>	61.21 <sub>3.76</sub>	53.91 <sub>4.55</sub>	79.23 <sub>3.00</sub>
DTFDMIL [27]	78.49 <sub>4.91</sub>	76.57 <sub>4.12</sub>	81.84 <sub>1.04</sub>	64.94 <sub>1.91</sub>	57.79 <sub>5.33</sub>	80.73 <sub>1.40</sub>
Fillioux et al. [8]	78.29 <sub>4.49</sub>	75.88 <sub>3.86</sub>	79.41 <sub>1.73</sub>	62.36 <sub>1.70</sub>	54.08 <sub>2.57</sub>	76.75 <sub>1.41</sub>
<b>MamMIL (Ours)</b>	<b>81.78</b> <sub>0.87</sub>	<b>80.15</b> <sub>0.69</sub>	<b>82.92</b> <sub>0.56</sub>	<u>65.23</u> <sub>4.77</sub>	<b>59.34</b> <sub>8.58</sub>	<b>84.23</b> <sub>2.10</sub>

a 1D sequence. By removing the padding and copying back the class token, we can obtain a 1D instance sequence that incorporates 2D spatial information as the output of the 2D-CAB.

**WSI Classification and Loss Function** After discriminative instance dependency mining and instance feature aggregation with the  $L$  MIL-SSM modules, we utilize the class token as the bag feature for WSI classification with a linear projection activated by a softmax function. In the experiments, we use the cross entropy loss for the model optimization.

### 3 Experimental Results

#### 3.1 Datasets

Two public WSI datasets, Camelyon16 [16,2] and BRACS [3], are utilized. Camelyon16 is a dataset for breast cancer micro-metastasis detection, which is officially divided into 270 training and 129 test WSIs. We further divide the training WSIs into training and validation sets at a ratio of 2 : 1, and the official test WSIs are untouched for testing. BRCAS is a breast cancer subtyping dataset where each WSI is categorized into benign, atypical, and malignant tumors. BRCAS is officially divided into a training set of 395 WSIs, a validation set of 65 WSIs, and a test set of 87 WSIs. The official division is used for evaluation.

#### 3.2 Experimental Settings

All experiments are done with an RTX 3090 GPU. Codes are implemented with Pytorch 2.1.1. When splitting WSIs, background patches are discarded by grayscale thresholding. RAdam [17] optimizer is utilized with a fixed learning rate of  $10^{-4}$  and a weight decay of 0.05. Each model is trained for 250 epochs. The model with the highest validation AUC is used for testing. We run each

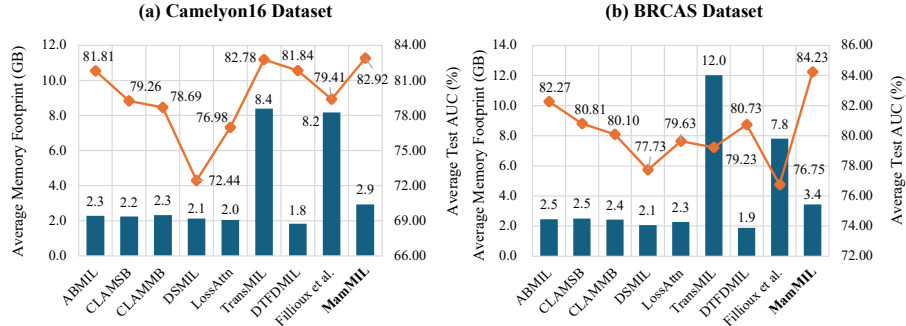


**Fig. 2.** GPU memory footprint comparison of MamMIL and SOTA methods. The blue bars demonstrate the average GPU memory occupation (GB), and the orange lines show the average test AUC of each method.

experiment with four seeds. Like most previous studies, AUC is utilized as the main evaluation metric. In addition, we report the accuracy and F1-Score with a classification threshold of 0.5. Due to the small training set of Camelyon16, we take the number of MIL-SSM modules as  $L = 1$  to avoid overfitting. For BRCAS, we take  $L = 2$ .

### 3.3 Comparison Results

**Classification Performance Comparison** The comparison results of MamMIL and other SOTA methods are shown in Table 1. The proposed MamMIL exceeds all SOTA methods in all metrics except the accuracy on BRCAS, which is slightly lower than ABMIL. Besides, we can see that MamMIL outperforms the SOTA methods on AUC with a larger margin for the BRCAS dataset than the Camelyon16 dataset. This may result from the fact that there are more training WSIs in the BRCAS dataset compared to Camelyon16. Therefore, the SSM blocks in MamMIL, which are proposed and optimized for large-scale data, are less likely to be overfitted. This phenomenon also implies that MamMIL may exhibit better performance if trained on large-scale datasets.

**GPU Memory Footprint Comparison** Except for the method proposed by Fillioux et al. [8], existing MIL frameworks either assume the instances in WSIs follow the i.i.d. assumption and use local attentions for instance aggregation (e.g., ABMIL and CLAM) or model the instance dependencies with global self-attention (e.g., TransMIL). The former approach requires a small amount of GPU memory, but their performance is usually limited. The latter approach usually performs better, but larger GPU memory is required. In contrast, MamMIL solves the conflict thanks to Mamba’s ability to model long sequences with linear complexity. As shown in Fig. 2, compared to TransMIL, the GPU memory

**Table 2.** Ablation studies on proposed components and class token positions.

Setting	Camelyon16			BRCAS		
	Accuracy	F1-Score	AUC	Accuracy	F1-Score	AUC
w/o Backward SSM	<u>81.01</u> <sub>1.69</sub>	79.44 <sub>1.30</sub>	80.93 <sub>1.62</sub>	62.07 <sub>1.15</sub>	53.43 <sub>2.96</sub>	81.23 <sub>0.47</sub>
w/o 2D-CAB	<u>81.01</u> <sub>1.40</sub>	79.43 <sub>1.46</sub>	<u>82.29</u> <sub>0.45</sub>	62.64 <sub>3.68</sub>	53.90 <sub>5.32</sub>	<u>83.95</u> <sub>1.68</sub>
w/o Shuffle	58.53 <sub>2.48</sub>	40.23 <sub>1.17</sub>	44.58 <sub>2.06</sub>	44.25 <sub>2.63</sub>	39.46 <sub>3.80</sub>	59.96 <sub>4.07</sub>
w/o CLS	<b>81.78</b> <sub>1.60</sub>	<u>79.99</u> <sub>1.85</sub>	81.42 <sub>0.74</sub>	<u>64.37</u> <sub>2.15</sub>	<b>62.30</b> <sub>1.38</sub>	82.25 <sub>0.63</sub>
First CLS	62.02 <sub>0.00</sub>	38.28 <sub>0.00</sub>	53.42 <sub>0.85</sub>	36.78 <sub>0.00</sub>	17.93 <sub>0.00</sub>	49.61 <sub>3.18</sub>
Middle CLS	78.49 <sub>2.76</sub>	76.30 <sub>2.74</sub>	77.60 <sub>2.57</sub>	63.22 <sub>2.15</sub>	58.97 <sub>4.44</sub>	82.39 <sub>0.91</sub>
<b>MamMIL (Ours)</b>	<b>81.78</b> <sub>0.87</sub>	<b>80.15</b> <sub>0.69</sub>	<b>82.92</b> <sub>0.56</sub>	<b>65.23</b> <sub>4.77</sub>	<u>59.34</u> <sub>8.58</sub>	<b>84.23</b> <sub>2.10</sub>

occupied by MamMIL is reduced by 65.5% and 71.7% on Camelyon16 and BRCAS, respectively. Besides, the memory footprint of MamMIL is lower than the S4D-based counterpart [8] as well, since complex-valued parameters are utilized in the S4D-based method, but Mamba only needs real-valued weights. In conclusion, the GPU memory occupation of Mamba is comparable to those frameworks with i.i.d. assumption, with a difference of less than 1.6 GB.

### 3.4 Ablation Studies

**Effects of Proposed Components** To verify the effectiveness of the proposed components, we perform ablation studies with results listed in Table 2. As we can see, all proposed components can improve model performance. Among them, the shuffle operation has the greatest impact on MamMIL’s performance. It may be because the shuffle operation can prevent the model from memorizing the fixed patterns in the limited training data, thereby avoiding overfitting. Besides, using both forward and backward SSMs can improve performance, as it solves the problem that SSMs can only model sequences unidirectionally. 2D-CAB can improve model performance as well, demonstrating the effectiveness of enabling MamMIL to perceive the 2D spatial relationships of the instances.

**Effects of Class Token Positions** Considering the latent state in SSM is a compression of previous input instances [10], to fuse all instance information into the class token, we add it at the last position of the feature sequence. Ablation studies are conducted to verify the effectiveness. As shown in Table 2, if the class token is placed in the first position, the model is almost unable to be trained, since SSMs scan and aggregate features sequentially from the beginning to the end. The performance of adding the class token in the middle or not using the class token (using average pooling to get the bag feature) is comparable for the two datasets, but both perform weaker than our proposed approach in AUC. In summary, putting the class token in the last position can achieve better overall performance in both datasets.



## 4 Conclusion

Considering the quadratic complexity of self-attention, current MIL frameworks based on the Transformer are forced to utilize linear attention for giga-pixelated WSI classification, which inevitably hinders model performance. To this end, we propose MamMIL, which is the first to introduce Mamba into MIL and enables efficient WSI classification with linear complexity. To address the disadvantages that Mamba only models sequences unidirectionally and cannot perceive 2D spatial relationships, we further introduce a Bi-SSM and a 2D-CAB block. Experiments validate that MamMIL achieves SOTA performance while consuming less GPU memory than existing methods based on the Transformer. In the future, MamMIL will be trained on large-scale datasets due to its high efficiency, and it is expected to show better performance.

## References

1. Acs, B., Hartman, J.: Next generation pathology: artificial intelligence enhances histopathology practice. *The Journal of pathology* **250**(1), 7–8 (2020)
2. Bejnordi, B.E., Veta, M., Van Diest, P.J., Van Ginneken, B., Karssemeijer, N., Litjens, G., Van Der Laak, J.A., Hermsen, M., Manson, Q.F., Balkenhol, M., et al.: Diagnostic assessment of deep learning algorithms for detection of lymph node metastases in women with breast cancer. *Jama* **318**(22), 2199–2210 (2017)
3. Brancati, N., Anniciello, A.M., Pati, P., Riccio, D., Scognamiglio, G., Jaume, G., De Pietro, G., Di Bonito, M., Foncubierto, A., Botti, G., et al.: Bracs: A dataset for breast carcinoma subtyping in h&e histology images. *Database* **2022**, baac093 (2022)
4. Chen, R.J., Lu, M.Y., Shaban, M., Chen, C., Chen, T.Y., Williamson, D.F.K., Mahmood, F.: Whole slide images are 2d point clouds: Context-aware survival prediction using patch-based graph convolutional networks. In: de Bruijne, M., Cattin, P.C., Cotin, S., Padoy, N., Speidel, S., Zheng, Y., Essert, C. (eds.) *Medical Image Computing and Computer Assisted Intervention – MICCAI 2021*. pp. 339–349. Springer International Publishing, Cham (2021)
5. Deng, J., Dong, W., Socher, R., Li, L.J., Li, K., Fei-Fei, L.: Imagenet: A large-scale hierarchical image database. In: *2009 IEEE Conference on Computer Vision and Pattern Recognition*. pp. 248–255 (2009)
6. Duman Keles, F., Wijewardena, P.M., Hegde, C.: On the computational complexity of self-attention. In: Agrawal, S., Orabona, F. (eds.) *Proceedings of The 34th International Conference on Algorithmic Learning Theory*. vol. 201, pp. 597–619. PMLR (2023)
7. Evans, A.J., Bauer, T.W., Bui, M.M., Cornish, T.C., Duncan, H., Glassy, E.F., Hipp, J., McGee, R.S., Murphy, D., Myers, C., et al.: Us food and drug administration approval of whole slide imaging for primary diagnosis: a key milestone is reached and new questions are raised. *Archives of pathology & laboratory medicine* **142**(11), 1383–1387 (2018)
8. Fillioux, L., Boyd, J., Vakalopoulou, M., Cournède, P.h., Christodoulidis, S.: Structured state space models for multiple instance learning in digital pathology. In: Greenspan, H., Madabhushi, A., Mousavi, P., Salcudean, S., Duncan, J., Syeda-Mahmood, T., Taylor, R. (eds.) *Medical Image Computing and Computer Assisted*

- Intervention – MICCAI 2023. pp. 594–604. Springer Nature Switzerland, Cham (2023)
9. Gadermayr, M., Tschuchnig, M.: Multiple instance learning for digital pathology: A review of the state-of-the-art, limitations & future potential. *Computerized Medical Imaging and Graphics* p. 102337 (2024)
  10. Gu, A., Dao, T.: Mamba: Linear-time sequence modeling with selective state spaces (2023)
  11. Gu, A., Goel, K., Gupta, A., Ré, C.: On the parameterization and initialization of diagonal state space models. In: Oh, A.H., Agarwal, A., Belgrave, D., Cho, K. (eds.) *Advances in Neural Information Processing Systems* (2022)
  12. He, K., Zhang, X., Ren, S., Sun, J.: Deep residual learning for image recognition. In: *2016 IEEE Conference on Computer Vision and Pattern Recognition (CVPR)*. pp. 770–778 (2016)
  13. Hosseini, M.S., Bejnordi, B.E., Trinh, V.Q.H., Chan, L., Hasan, D., Li, X., Yang, S., Kim, T., Zhang, H., Wu, T., et al.: Computational pathology: a survey review and the way forward. *Journal of Pathology Informatics* p. 100357 (2024)
  14. Ilse, M., Tomczak, J., Welling, M.: Attention-based deep multiple instance learning. In: Dy, J., Krause, A. (eds.) *Proceedings of the 35th International Conference on Machine Learning*. vol. 80, pp. 2127–2136. PMLR (2018)
  15. Li, B., Li, Y., Eliceiri, K.W.: Dual-stream multiple instance learning network for whole slide image classification with self-supervised contrastive learning. In: *Proceedings of the IEEE/CVF Conference on Computer Vision and Pattern Recognition (CVPR)*. pp. 14318–14328 (2021)
  16. Litjens, G., Bandi, P., Ehteshami Bejnordi, B., Geessink, O., Balkenhol, M., Bult, P., Halilovic, A., Hermsen, M., van de Loo, R., Vogels, R., et al.: 1399 h&e-stained sentinel lymph node sections of breast cancer patients: the camelyon dataset. *Giga-Science* **7**(6), giy065 (2018)
  17. Liu, L., Jiang, H., He, P., Chen, W., Liu, X., Gao, J., Han, J.: On the variance of the adaptive learning rate and beyond (2021)
  18. Liu, Y., Tian, Y., Zhao, Y., Yu, H., Xie, L., Wang, Y., Ye, Q., Liu, Y.: Vmamba: Visual state space model (2024)
  19. Lu, M.Y., Williamson, D.F., Chen, T.Y., Chen, R.J., Barbieri, M., Mahmood, F.: Data-efficient and weakly supervised computational pathology on whole-slide images. *Nature biomedical engineering* **5**(6), 555–570 (2021)
  20. Qu, L., Luo, X., Liu, S., Wang, M., Song, Z.: Dgmil: Distribution guided multiple instance learning for whole slide image classification. In: Wang, L., Dou, Q., Fletcher, P.T., Speidel, S., Li, S. (eds.) *Medical Image Computing and Computer Assisted Intervention – MICCAI 2022*. pp. 24–34. Springer Nature Switzerland, Cham (2022)
  21. Ruan, J., Xiang, S.: Vm-unet: Vision mamba unet for medical image segmentation (2024)
  22. Shao, Z., Bian, H., Chen, Y., Wang, Y., Zhang, J., Ji, X., zhang, y.: Transmil: Transformer based correlated multiple instance learning for whole slide image classification. In: Ranzato, M., Beygelzimer, A., Dauphin, Y., Liang, P., Vaughan, J.W. (eds.) *Advances in Neural Information Processing Systems*. vol. 34, pp. 2136–2147. Curran Associates, Inc. (2021)
  23. Shi, X., Xing, F., Xie, Y., Zhang, Z., Cui, L., Yang, L.: Loss-based attention for deep multiple instance learning. In: *Proceedings of the AAAI conference on artificial intelligence*. vol. 34, pp. 5742–5749 (2020)
  24. Song, A.H., Jaume, G., Williamson, D.F., Lu, M.Y., Vaidya, A., Miller, T.R., Mahmood, F.: Artificial intelligence for digital and computational pathology. *Nature Reviews Bioengineering* **1**(12), 930–949 (2023)

25. Vaswani, A., Shazeer, N., Parmar, N., Uszkoreit, J., Jones, L., Gomez, A.N., Kaiser, L., Polosukhin, I.: Attention is all you need. In: Proceedings of the 31st International Conference on Neural Information Processing Systems. p. 6000–6010. NIPS’17, Curran Associates Inc., Red Hook, NY, USA (2017)
26. Xiong, Y., Zeng, Z., Chakraborty, R., Tan, M., Fung, G., Li, Y., Singh, V.: Nyströmformer: A nyström-based algorithm for approximating self-attention. In: Proceedings of the AAAI Conference on Artificial Intelligence. vol. 35, pp. 14138–14148 (2021)
27. Zhang, H., Meng, Y., Zhao, Y., Qiao, Y., Yang, X., Coupland, S.E., Zheng, Y.: Dtf-d-mil: Double-tier feature distillation multiple instance learning for histopathology whole slide image classification. In: Proceedings of the IEEE/CVF Conference on Computer Vision and Pattern Recognition (CVPR). pp. 18802–18812 (2022)
28. Zhu, L., Liao, B., Zhang, Q., Wang, X., Liu, W., Wang, X.: Vision mamba: Efficient visual representation learning with bidirectional state space model (2024)